Preparation, characterization and dynamical mechanical properties of dextran-coated iron oxide nanoparticles (DIONPs)

Hatice Kaplan Can, Serap Kavlak, Shahed ParviziKhosroshahi & Ali Güner

Published online: 20 Apr 2017.

Submit your article to this journal

View related articles

View Crossmark data

Taylor & Francis
Taylor & Francis Group

Check for updates

Preparation, characterization and dynamical mechanical properties of dextran-coated iron oxide nanoparticles (DIONPs)

Hatice Kaplan Can, Serap Kavlak, Shahed ParviziKhosroshahi and Ali Güner

Department of Chemistry, Faculty of Science, Division of Polymer Chemistry, Hacettepe University, Ankara, Turkey

ABSTRACT

Dextran-coated iron oxide nanoparticles (DIONPs) with appropriate surface chemistry exhibit many interesting properties that can be exploited in a variety of biomedical applications such as magnetic resonance imaging (MRI) contrast enhancement, tissue repair, hyperthermia, drug delivery and in cell separation. This paper reports the experimental detail for preparation, characterization and investigation of thermal and dynamical mechanical characteristics of the dextran-coated Fe_3O_4 magnetic nanoparticles. In our work, DIONPs were prepared in a 1:2 ratio of Fe(II) and Fe(III) salt in the HCl solution with NaOH at given temperature. The obtained dextran-coated iron-oxide nanoparticles structure–property correlation was characterized by spectroscopic methods; attenuated total reflectance-Fourier transform infrared spectroscopy (ATR-FTIR) and XRD. Coating dextran on the iron-oxide proof of important peaks can be seen from the ATR-FTIR. Dramatic crystallinity increment can be observed from the XRD pattern of the iron-oxide dextran nanoparticles. The thermal analysis was examined by differential scanning calorimetry (DSC), thermal gravimetric analysis (TGA) and differential thermal analysis (DTA). Dynamical mechanical properties of dextran nanoparticles were analysed by dynamic mechanical analysis (DMA). Thermal stability of the iron oxide dextran nanoparticles is higher than that of the dextran.

Introduction

Iron oxide nanoparticles (IONPs) have been studied extensively over the past few decades to fabricate various novel contrast agents. Nano-sized Fe_3O_4 (magnetite) is an important member of spinel type ferrite. Based on their unique mesoscopic physical, thermal, mechanical and chemical properties; magnetic nanoparticles are one of the best candidates for multiple *in vivo* biomedical applications such as tissue repair, cellular therapy such as cell labelling, targeting and as a tool for cell-biology research to separate and purify cell populations, magnetic fluids-guided carriers for localizing drugs or radioactive therapies, magnetic storage, tumor hyperthermia and magnetic resonance imaging (MRI) [1–8]. All of these biomedical applications require that the nanoparticles have high magnetization values, a size smaller than 100 nm, and a narrow particle size distribution. By another word, the control of the monodisperse size is very important because the physical and chemical properties of nanoparticles are strongly under the influence of these properties. Therewith, the major advantage of using particles with this size is ability to easier attachment of ligands (their higher effective surface areas), high stability (lower sedimentation rates) and improved tissue diffusion. As well as, special surface coating of the magnetic particles require, which has to be not only non-toxic and biocompatible but also allow a targetable delivery with particle localization in a specific area. Magnetic nanoparticles can be glue to different molecules such as: enzymes, proteins, drugs

or nucleotides antibodies. In addition, nanoparticles can be directed to a tissue, organ, and can be directed to an organ tumour web using an external magnetic field [9,10]. For biocompatible usage, iron oxide nanoparticles are the best choice because of their biological, superparamagnetic behaviour and good chemical stability [11].

The nanostructure is based on an inorganic core of iron oxide (γ-Fe_2O_3, Fe_3O_4), coated with some polymers such as dextran, chitosan, poly(ethylenimine) (PEI) and poly(ethylene glycol) (PEG) [12–14]. Dextran is a polysaccharide $(C_6H_{10}O_5)_n$, composed exclusively of alpha-D (1–6) linkages with some unusual 1,3 glucosides linkages at branching points. Dextrans are used to coat iron oxide nanoparticles in aqueous solution.

The first report of the formation of magnetite in the presence of dextran was by Molday and Mackenzie [15]. As noted above derivative of dextran-coated magnetic nanoparticles are a powerful platform for these applications [16]. According to pharmacokinetic and toxicity studies, the derivative of dextran has revealed these nanomaterials can be sufficiently non-toxic, biodegradable [17,18] and extended vascular retention times. On the other side, dextran-coated iron oxide nanoparticles (DIONPs) are a well-established platform for the synthesis of multifunctional imaging agents [19]. These include monocrystalline iron oxide nanoparticles [20]. Some nanoparticles with iron cores and carbohydrate coatings have been approved for human usage. The US Food and Drug Administration (FDA) in 1996, approbate as the first nanoparticle-based iron oxide imaging agent for the detection of liver

lesions. A smaller monodisperse version, Combidex has been used to image occult prostate cancer lymph-node metastases in humans.

Various methods have been developed for the preparation of iron oxide nanoparticles such as: co-precipitation method; hydrothermal synthesis techniques are an alternative method for the preparation of highly crystalline iron oxide nanoparticles, microemulsion and inverse microemulsion, thermal decomposition of organic precursors, sol–gel technique, wet grinding method, reduction of hematite by CO/CO_2, γ-ray radiation, hydrolysis and oxidation of $Fe(OH)_2$ by H_2O_2 [21–29]. In order to design nanoparticles for specific applications, surface structure, atomic structure of the particle and its magnetic structure or spin dynamics should be known. Specifically, for metallic nanoparticles this includes understanding atomic symmetry and chemistry of the interior atoms and surface atoms, as well as the dynamics of both interior and surface spins. For the case of iron oxide nanoparticles, the surface energy and synthesis methodology may also lead to the stabilization of defects [30].

This work expresses the effort to understand the preparation of DIONPs in situ co-precipitation methods and nature of the interaction mechanism and thermal stability of dextran with iron oxide. This study describes the synthesis route of DIONPs and physical properties characterization by using XRD and attenuated total reflectance-Fourier transform infrared spectroscopy (ATR-FTIR). The thermal analysis was examined by differential scanning calorimetry (DSC), differential thermal analysis (DTA) and thermal gravimetric analysis (TGA). Dynamical mechanical properties of magnetic dextran nanoparticles were analysed by dynamic mechanical analysis (DMA).

Materials and methods

Materials

All chemicals used were of reagent without further purification. Ferrous chloride tetrahydrate ($FeCl_2 \cdot 4H_2O$), ferric chloride ($FeCl_3 \cdot 6H_2O$), aqueous ammonia, hydrochloric acid (HCl), nitric acid (HNO_3) and dextran (molecular weight $\sim$40000) are purchased from Sigma-Aldrich. De-ionized water was used in the synthesis of nanoparticles and in the rinsing of clusters.

Synthesis of iron-oxide dextran nanoparticles

Iron-oxide nanoparticles were prepared by co-precipitation method which is probably the simplest and offers some advantages: simple and rapid preparation, easy control of particle size and composition, various possibilities to modify the particle surface state allowing making homogenous and stable dispersions in liquid or solid media. Iron oxides (Fe_3O_4 or γFe_2O_3) are usually prepared by an aging stoichiometric mixture of ferrous and ferric salts in aqueous medium. Ferric chloride hexahydrate ($FeCl_3 \cdot 6H_2O$) and ferrous chloride tetrahydrate ($FeCl_2 \cdot 4H_2O$), in the 2M HCl were mixed at 95 °C ($Fe^{2+}/Fe^{3+} = \frac{1}{2}$). After this process, the mixture was dropped into 220 ml of NaOH (2.2 mol/l) solution under vigorous stirring for about 35 min. Black precipitate immediately formed and the precipitate of magnetite was transformed into γ-Fe_2O_3 particles by repeated treatment with HNO_3 (2.0 mol/l) and $FeNO_3$ (0.3 mol/l) solutions (Scheme 1). The acidic precipitate was isolated by decantation on a magnet, separated by centrifugation (6000 rpm), then washed in acetone and dispersed in deionized water.

Dextran solution (20 g/100 ml water) was heated for 1 h at 90 °C with successive mixing (250 rpm/min). In this time, 40 ml of 5 M NaOH was added to the solution. Ferrite solution (30 ml) containing stoichiometric ratio of 1:2 of $FeCl_3 \cdot 6H_2O$ and $FeCl_2 \cdot 4H_2O$ was added dropwise to the solution. The suspension was incubated for 1 h at 95 °C with mild stirring. The 5 M NaOH was added dropwise to generate a pH of 11. The precipitate was centrifuged and washed with deionized water. The product was separated by centrifugation (1000 rpm) and dried at 45 °C (Scheme 1).

Characterization of iron-oxide dextran nanoparticles

X-ray diffraction (XRD)

The X-ray diffraction, (XRD) patterns were obtained from a Rigaku D-Max 2200 powder diffractometer. The XRD diffractograms were measured at 2θ, in the range 2–50°, using a Cu-Kα incident beam $\lambda = 1.54059$ A°), monochromated by a Ni-filter. The scanning speed was 1°/min, and the voltage and current of the X-ray tubes were 40 kV and 30 mA, respectively. The Bragg equation was used to calculate the interlayer spacing (d) $n\lambda = (2d \sin\theta)$, where n is the order of reflection, and θ is the angle of reflection. Crystallinity of the nanocomposites was calculated using the Equations (1) and (2)

$$X_c = \frac{\int_0^\infty s^2 I_c(s)d}{\int_0^\infty s^2 I(s)d} \quad (1)$$

where s is the magnitude of the reciprocal-lattice vector which is given by $s = (2\sin\theta)/\lambda$ (θ is one-half the angle of
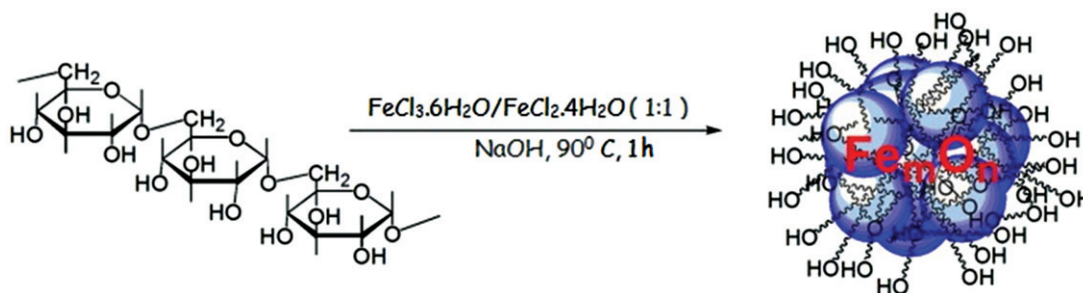
Scheme 1. The preparation pathway of DIONPs.

deviation of the diffracted rays from the incident X-rays, and λ is the wavelength); $I(s)$ and $I_c(s)$ are the intensities of coherent X-ray scattering from both crystalline and amorphous regions and from only crystalline region of polymer sample, respectively,

$$\%X_c = \frac{W_c}{W_c + W_a} \times 100 \qquad (2)$$

where W_c and W_a are the areas of the crystalline and amorphous portions in the X-ray patterns, respectively.

Attenuated total reflectance-Fourier transform infrared spectroscopy (ATR-FTIR)

ATR-FTIR spectra of dextran-iron oxide magnetic nanoparticles and were taken with a Mattson FTIR spectrophotometer in the 4000–400 cm^{-1} range where 30 scans were taken at 4 cm^{-1} resolution.

Differential thermal analysis (DTA) and thermal gravimetric analysis (TGA)

DTA and TGA of the dextran-iron oxide magnetic nanoparticles were recorded using Shimadzu DTG-60 H thermal analyser in dynamic nitrogen atmosphere (100 ml/min) at a heating rate of 10 °C/min, in platinum crucibles as sample vessel, using α-Al$_2$O$_3$ as reference.

Dynamic mechanic analysis (DMA)

Dynamic mechanic behaviours of dextran and dextran-iron oxide magnetic nanoparticles were analysed by Dynamic Mechanic Analyser (DMA Q800, TA Instruments). Dextran and dextran-iron oxide nanoparticles (mixed with Al$_2$O$_3$, 50:50 wt. %) were put into the power holder of DMA and then temperature dependences were measured (3 °C/min at 1 Hz). The storage modulus (E$'$), loss modulus (E$''$), damping factor (tan δ = E$''$/E$'$), dynamic force (DF), complex modulus (CM), dynamic viscosity (DV) and complex viscosity (CV) were recorded with increasing temperature for dextran and dextran-modified iron oxide magnetic nanoparticles at the same conditions.

Results and discussion

Characterization of iron-oxide dextran nanoparticles by ATR-FTIR

DIONPs were prepared by co-precipitation methods in alkaline medium. Figure 1 shows the ATR-FTIR spectra of the (a) dextran (b) dextran coated-iron oxide magnetic nanoparticles. In region of 3600–1600 cm^{-1} bands appear: a broad band centered at 3363 cm^{-1} and 1650 cm^{-1} assigned to the OH stretching ν(O–H) and H–O–H (δ O–H) vibrational bands due to adsorbed water molecules in the sample the weak signal at 2860 cm^{-1} [31]. The band at 1451 cm^{-1} may be due to C–O–H deformation vibration with contributions of O–C–O symmetric stretching vibration of carboxylate group [32]. The stronger peaks appear in the range of 1155–866 cm^{-1} mainly attributed to the stretching vibration of C–O–C [33]. The spectrum shows one mode around 1014 cm^{-1} assigned to the ν(C–O) stretching mode in the ring [34]. Peak intensities and positions at 915, 866, 765 cm^{-1} in the ATR-FTIR spectrum display the characteristic absorptions of dextran (α1, 3 of glycoside unit). The bands observed in the 687 cm^{-1}
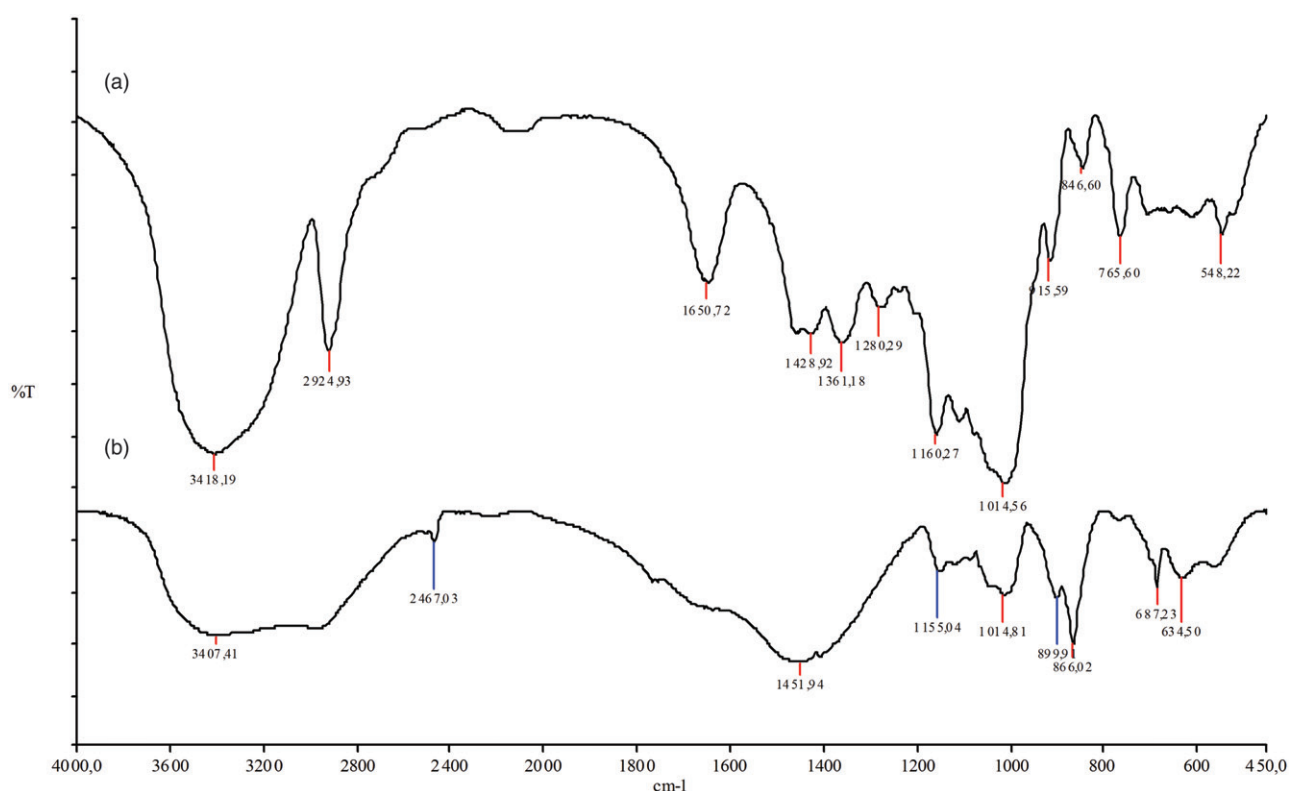

**Figure 1.** ATR-FTIR spectra of the (a) dextran and (b) DIONPs.

corresponds to the Fe–O vibrations modes of γ-Fe_2O_3 of octahedral structure, and the bands in the $450\,cm^{-1}$ assigned the Fe–O vibrations modes of tetrahedral structure. Iron oxide particles also show O–H absorption at about $3500\,cm^{-1}$ due to the physically absorbed water molecules. The results of ATR-FTIR are accordance with the literature [35] for the dextran coating and iron oxide nanoparticle [36]. The coating mechanism on iron oxide can be enlightened depending on the ATR-FTIR peak assignments. After coating some significant band shifts can be observed especially in the region below $1000\,cm^{-1}$. The absorption of dextran on the iron-oxide proof can be seen in the DIONPs 2920, 1420 and $1401\,cm^{-1}$ peaks assigned to the dextran molecule ν(C–H) and δ(C–H) vibrational modes (Figure 1(b)).

Taking into considerations of ATR-FTIR spectroscopically results, this coating most probable mechanism can be proposed by hydrogen bonding of the dextran hydroxyl groups and iron oxide particle surface (Scheme 2). Water lies in between the dextran and iron oxide surface forming inter- and intramolecular hydrogen bonds [37]. This can be explained by O–H bands merging and broadening at the $\sim$3400 cm^{-1}. In the region between 1500 and 1000 cm^{-1} peaks of free dextran are reduced after coating. Polar reactive

groups between the oxide and dextran atoms form to physically interactions.

Characterization of iron-oxide dextran nanoparticles by XRD

The XRD patterns of dextran (a) and DIONPs (b) can be seen from the Figure 2. A series of characteristic peaks were observed in the XRD pattern at 2θ of 30.1, 34, 42, 53.4, 55 and 62.7 marked by their indices of 220, 311, 400, 422, 511, 440 crystal faces of Fe_3O_4 spinel structure (Figure 2(a,b)) [28]. The refinement of XRD spectra indicated that no other phases except the maghemite are detectable. The positions and relative intensities of the reflection peak of MNPs agree with the XRD diffraction peaks of standard Fe_3O_4 samples indicating that the black-coloured magnetic powders are magnetite nanoparticles that agree well with the literature [38]. Sharp peaks also suggest that the Fe_3O_4 nanoparticles have good crystallized structure. Peak broadening observed is consistent with the small particle size. It was found that the magnetite crystallites could be well indexed to the inverse cubic spinel structure of Fe_3O_4 [39,40]. The distance between layers in the crystal structure d (nm) values of was calculated according to
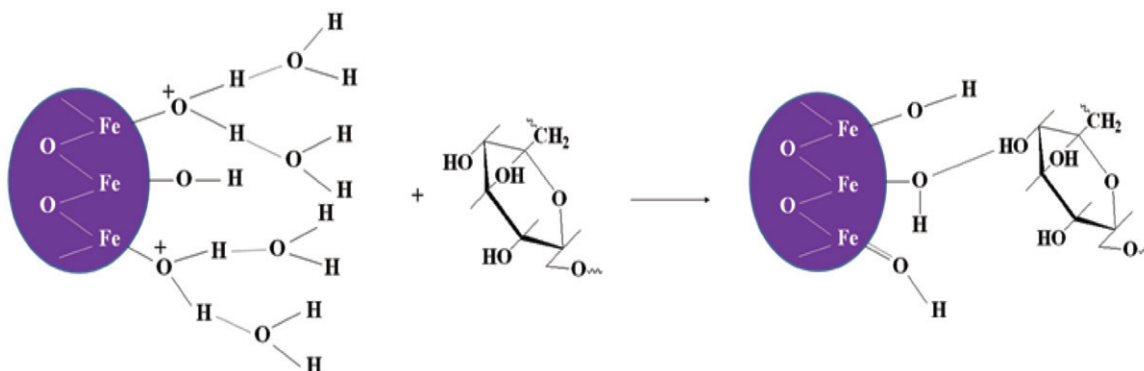
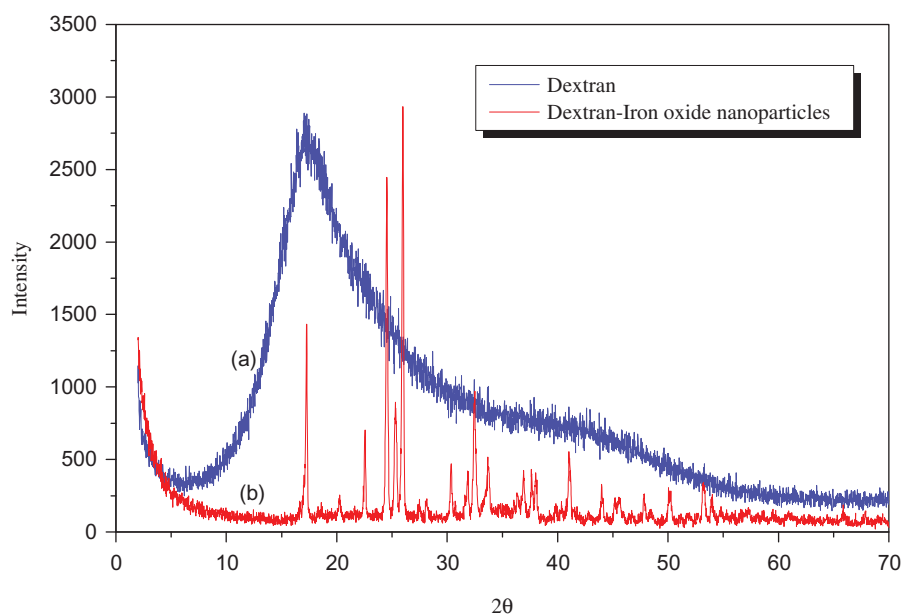**Scheme 2.** Proposed dextran coating mechanism of nanoparticles via hydrogen bonding.

**Figure 2.** The X-ray diffraction patterns of samples prepared: dextran (a) and DIONPs (b).

Table 1. XRD parameters of dextran and DIONPs.

2θ	The distance between layers in the crystal structure d (nm)	Crystalline form
65	1.4336	Fe
45	2.0069	Fe
43	2.0607	FeO
36	2.4700	FeO
37	2.4455	Fe_2O_3
33	2.7578	Fe_2O_3
56	1.6414	Fe_3O_4
45	1.9910	Fe_3O_4

the Bragg law [41]. The d values are given in Table 1. The distance between layers in the crystal structure d (nm) are attributed the crystal form of Fe, FeO, Fe_2O_3 and Fe_3O_4. A series of characteristics crystal peaks and d values indicate the dextran-coated nanoparticles were prepared successfully [42]. Using XRD patterns of dextran and dextran nanoparticles according to the equation, 4% crystallinity (% X_c) was calculated. Amorphous character of the dextran homopolymer (% $X_c = 2.11$) change to the semi-crystalline structure when the iron oxide coating in dextran iron nanoparticles (% $X_c = 22.83$) (Figure 2). This dramatic change in crystallinity can be explained the iron oxide crystal structures [41].

Characterization of iron-oxide dextran nanoparticles by thermal methods

The thermal stability of dextran and dextran-coated nanoparticles was identified by TGA, DSC and DTA method. Thermal degradation of studied systems is complicated, so for easy following all curves (DSC, TGA and DSC) can be divided into three main ranges (I: 30–200 °C, II: 200–400 °C and III: 400–800 °C), even if any stage is composed of two or more less clear, overlapped processes. The thermogravimetric data were obtained from thermogravimetric analyser (TGA) performed under dry nitrogen atmosphere over a temperature range of 30 to 800 °C at a heating rate of 10 °C/min. Thermograms of dextran and DIONPs are shown in Figure 3. As can be seen from the Figure 3, the temperature of onset decomposition of dextran is lower than the dextran-coated nanoparticles. During heating up to the 800 °C temperature, the dextran shows two significant decomposition stages (Figure 3(a)). The first decomposition stage in the temperature range from 20 to 150 °C represents the water evolving. The weight loss of dextran is quite small (3%) because of the removal of absorbed physical and chemical water [39]. The second one in the temperature range of 250–350 °C with mass loss of 77% corresponds to the organic breakdown of polysaccharide dextran chains, the total mass loss up to 800 °C was. This weight loss in this stage is connected to the rupture of polysaccharide chains (including dehydration, deamination, deacetylation, breaking of glycoside bonds, and pyranose ring opening), vaporization, and elimination of degradation products [43]. There is no significant weight change from 400 to 800 °C, implying the within the temperature range. The thermal decomposition of dextran-coated nanoparticles occurs through three stages. The first stage is related to the physically absorbed water of dextran, second step decomposition corresponds to the dextran main chain
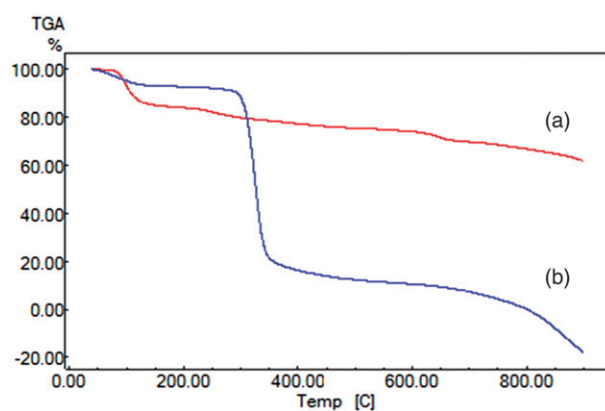
Figure 3. TGA thermograms of the (a) dextran and (b) DIONPs.
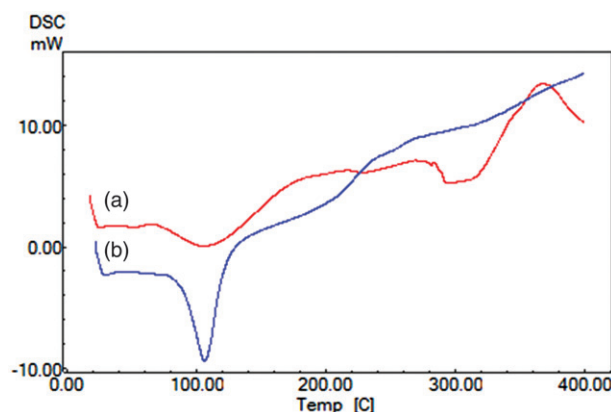
Figure 4. DSC thermograms of the (a) dextran and (b) dextran-iron oxide nanoparticles.

around 250–300 °C. When the dextran decomposed completely, the residual substance mostly is magnetic nanoparticles.

Figure 4 shows the DSC curves of dextran (Figure 4(a)) and dextran-iron oxide nanoparticles (Figure 4(b)) (DIONPs). In the case of pure dextran, the broad endothermic peak starting at 55 °C was ascribed to the water evolving or pseudo melting peak [44]. The glass transition temperature (T_g) of dextran was approximately 102 °C (Figure 4(a)), was almost the same as that of and dextran-coated magnetic nanoparticles, shown in Figure 4(b). At temperatures higher than 270 °C, the breakdown of the organic skeleton of dextran took place. The difference nature of the DSC between the dextran and dextran nanoparticles can be explained by the restricting effect of the presence of Fe_3O_4, magnetic nanoparticles in polymer matrix [36].

In order to analyse the nature of the bonding between the dextran and iron oxide and its evolution with temperature and to support the other thermal methods differential thermal analyses was used. DTA curves (Figure 5(a,b)) reveal that the energy is systematically released during thermal degradation of dextran and dextran-coated nanoparticles. Although the small peak can be seen for the dextran at 102 °C, the sharp transition peak belongs to the nanoparticles at the same temperature range. Small deflection on DTA curve corresponding to maximum rate of the last decomposing process is observed in two types of samples. The carbon

residue at 800 °C is almost the same in all studied polymer and polymer-iron oxide specimens. The results of DSC are agreeable with the DTA results seen in Figure 4. The nature of the curve showed that dextran was coated on the surface of Fe_3O_4 nanoparticles [37,45].

Characterization of iron-oxide dextran nanoparticles by DMA

DMA has been widely used for polymer and nanoparticles characterization for the investigation of segmental chain motions and for determining the viscoelastic character of polymers and nanoparticles from the glass to the rubber state over a specific range of temperature and oscillatory frequency. This technique also describes as the applying and oscillating force to a material and its response to that oscillating force [46] and it measures the stiffness and damping properties of a material and determines the E′, E″ and tan δ.
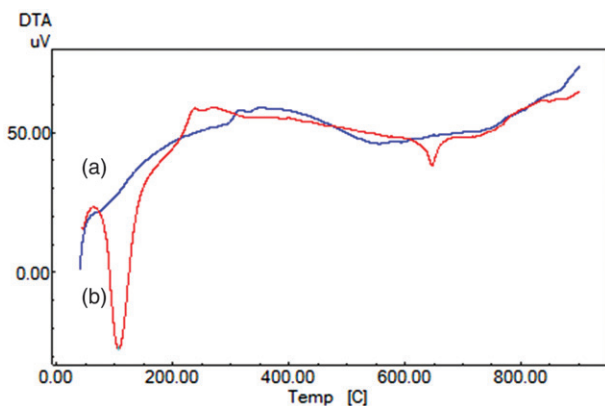

Figure 5. DTA thermograms of the (a) dextran and (b) dextran-iron oxide nanoparticles.

The dynamic mechanical properties of dextran and dextran-iron oxide nanoparticles were analysed by DMA (Figures 6–12). Limited studies were found in literature for the dynamical mechanical properties and analysis of dextran iron oxide nanoparticles. This study will be an important guidance and pathway in dynamic mechanical behaviour. The E′, E″ and tan δ of dextran and dextran-coated magnetic nanoparticles are shown in Figures 6–8. Storage modulus behaviour of dextran exhibits decreasing tendency with increasing temperature as the increased chain mobility of the dextran molecules and can be explained by the softening of the polymer. For the magnetic nanoparticles, the same behaviour was observed but the higher storage modulus than dextran sample as in the nanoparticles chain mobility of polymer was restricted because of the presence of iron oxide particles. In the loss modulus-temperature curves, same trend was observed as that of storage modulus and the peak maximum was increased with the modification of iron oxide with dextran. This may be explained by the interaction of the polar group, i.e. hydroxyl group of the dextran and iron oxide groups. This was also summarized at Table 2. In addition to storage and loss modulus, similar behaviour was observed for the tan δ curves with increasing temperature (47). The glass transition temperature (T_g) is usually described or accompany with a large number of chain segments motions of chains in polymer. There are several methods to determine the T_g, but DMA is the most sensitive method for the definition of the glass transition. For DMA; a temperature scans at constant frequency can generate a finger print of the material's relaxation process and its glass transition temperature (T_g). At Figures 6–8, the T_g values were observed at 70, 69, 69 °C for dextran and 73, 92, 93 °C for dextran-coated magnetic nanoparticles from the E′, E″ and tanδ, respectively. The higher T_g values for the dextran-coated nanoparticles may signify that the nanoparticles process stronger and this
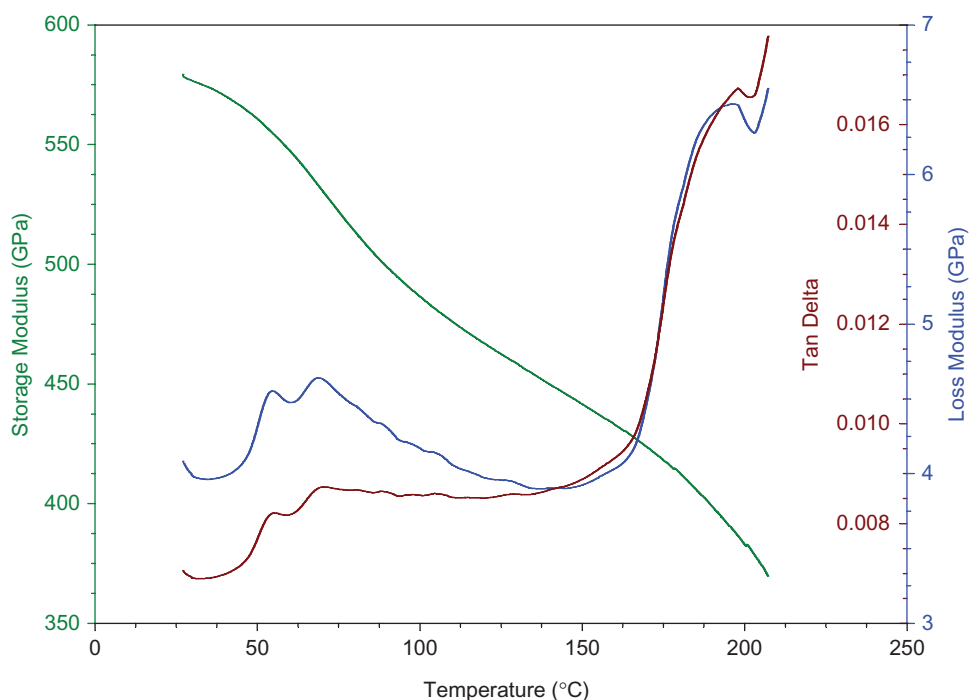

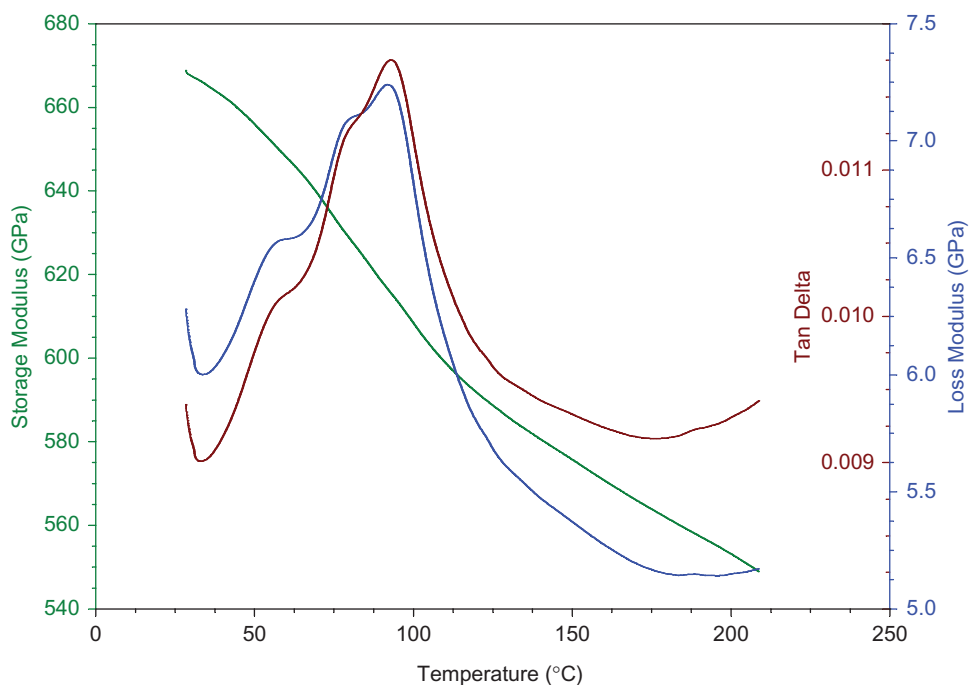**Figure 6.** DMA plots of dextran (E′, E″ and tan δ vs. T).

Figure 7. DMA plots of dextran-iron oxide nanoparticles (E′, E″ and tan δ *vs*. T).
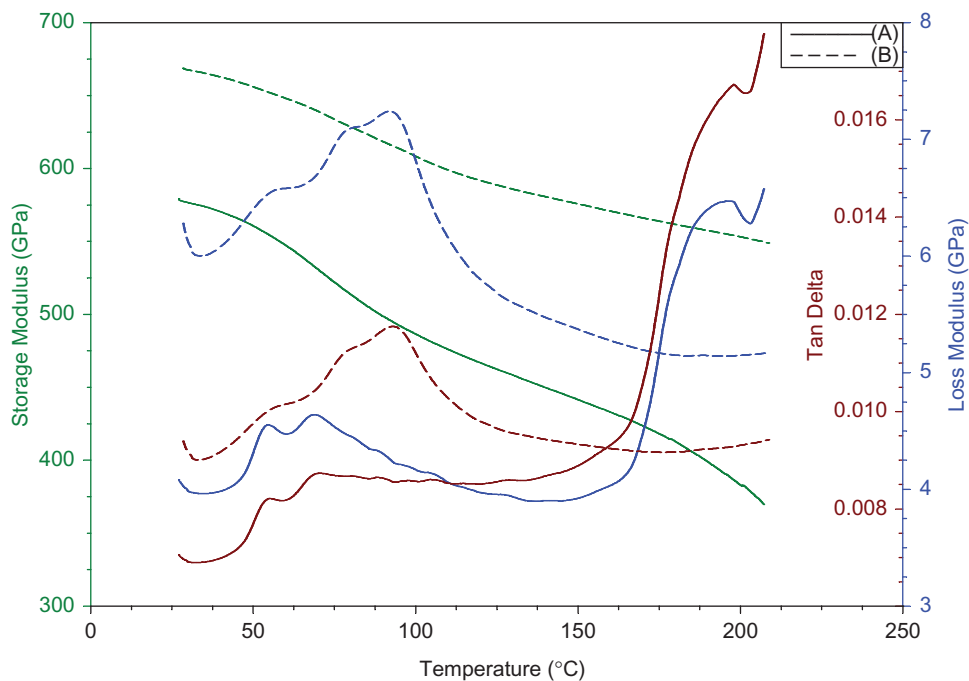

Figure 8. DMA plots: (A) dextran, (B) dextran-iron oxide nanoparticles.

behaviour also related with the interactions such as hydrogen bonding and dipole–dipole interactions due to its specific groups. In addition to glass transition peak, dextran-coated magnetic nanoparticles show a broad T_g peak with a shoulder at 80 °C at the loss modulus and tan δ plots and these appeared peaks may result from the interaction from the H-bonding between hydroxyl groups of dextran and iron oxide. On the other hand, according to loss modulus and tan δ curves of dextran, another transition was observed before T_g at 54 °C. The transition below T_g (sub-T_g transition) can be

associated by the motions of side chain groups or the evolving of the physically bound water. When compared the T_g values obtained by DSC, DTA and DMA, there is a small differences can be seen. The difference can be explained by the highest sensitivity of the DMA measurements [48]. Depending on measurements way of the T_g values, a significant difference observed between dextran and nanoparticles due to the nanoparticles formation was summarized at Table 3. As can be seen that after T_g values, differences were bigger as the formation of the nanostructure in the
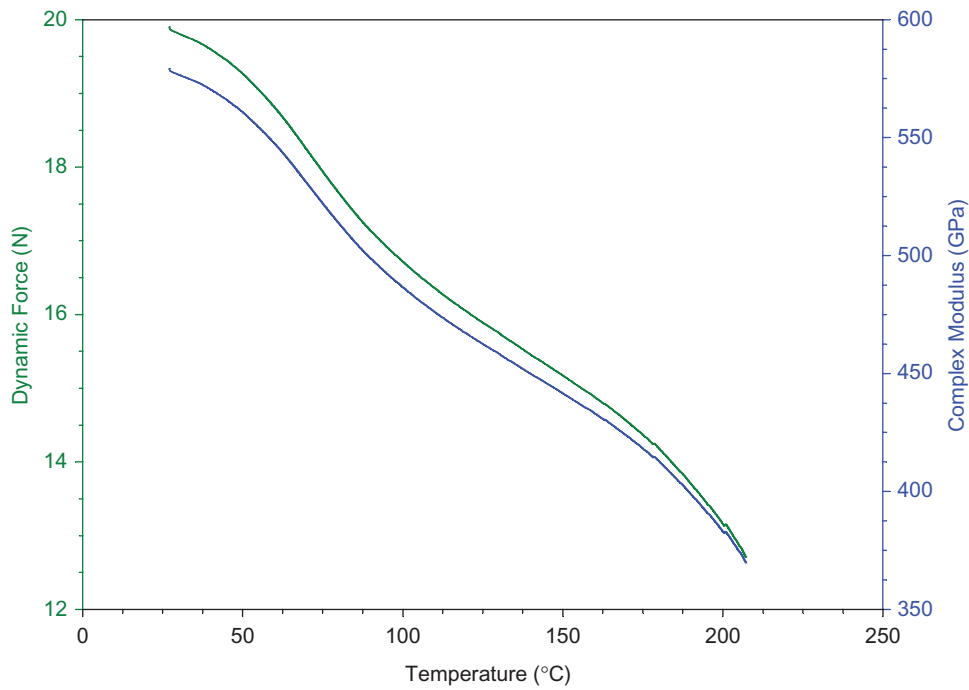
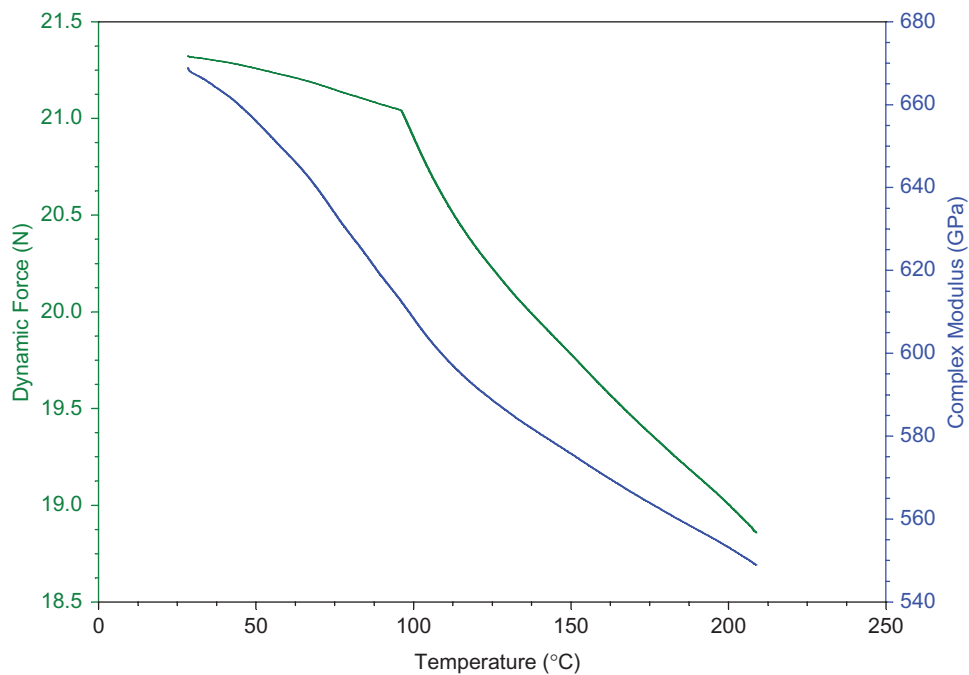**Figure 9.** DMA plots of dextran (DF and CM *vs.* T).

Figure 10. DMA plots of dextran-iron oxide nanoparticles (DF and CM *vs.* T).

nanoparticles. DMA curves of DF- and CM-T curves for dextran and nanoparticles are shown in Figures 9 and 10, and DV- and CV-T curves are shown in Figures 11 and 12. The difference between dynamic force (Δ) is 2.00 at 50 °C, 4.19 at 100 °C and 4.62 at 150 °C for the dextran and nanoparticles. Complex viscosity decreased with increasing temperature as expected. Dynamic viscosity increased up to 92 and 69 °C and then a peak viscosity was reached viscosity decreased with increasing temperature for the dextran-coated nanoparticles and dextran and this may because of the raptures of granules.

Conclusion

DIONPs were prepared by co-precipitation method by iron salts in the presence of dextran solution. Comparable peculiarities and coating mechanism of the dextran and DIONPs were enlightened by using ATR-FTIR. The ATR-FTIR results of the nanoparticles showed the presence of characteristic stretching bands proved a clear evidence for the formation of iron-oxide nanoparticles inside the polymer. The crystalline structure and patterns also were investigated by XRD. Thermal stability and structure relationship were examined by
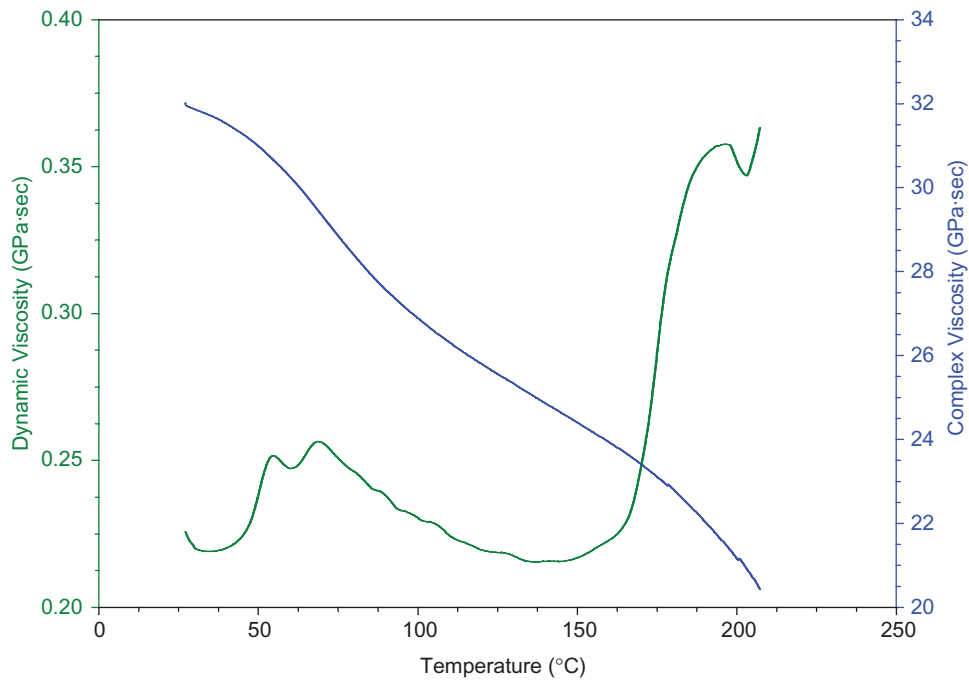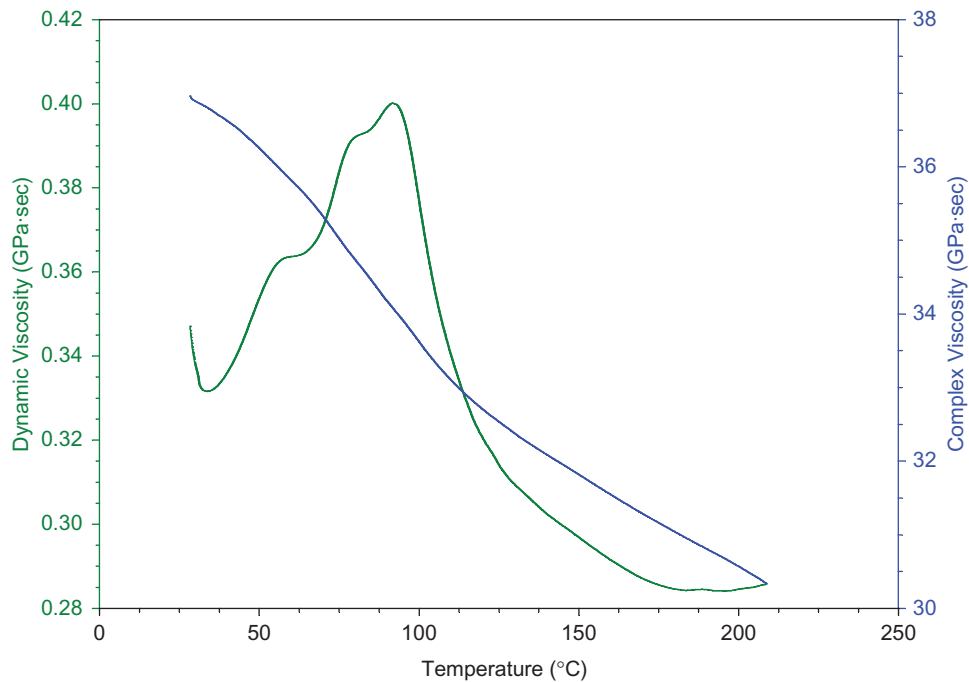
Figure 11. DMA plots of dextran (DV and CV *vs*. T).

Figure 12. DMA plots of dextran-iron oxide nanoparticles (DV and CV *vs*. T).

Table 2. Storage modulus (SM) and complex viscosity (CM)-temperature (T) results of dextran and dextran-iron oxide nanoparticles.

	SM (GPa) $\times 10^2$ at (°C) CV (GPa s) $\times 10^2$ at (°C)								
Polymer and nanoparticles	30	50	100	150	200	30	50	100	150	200
Dextran	5.77	5.61	4.87	4.42	3.83	0.32	0.31	0.27	0.24	0.21
Dextran-iron oxide nanoparticles	6.68	6.56	6.08	5.76	5.53	0.37	0.36	0.34	0.32	0.31

Table 3. DMA parameters [tan δ, dynamic force (DF) and $\Delta = (DF_n - DF_p)$] of dextran and dextran-iron oxide nanoparticles.

	Tan δ, (°C)			DF (N), (°C)			Δ (N), (°C)		
Polymer and nanoparticles	$T_{s\ (onset)}$	$T_{s\ (max)}$	T_g	50	100	150	50	100	150
Dextran	45	55	69	19.26	16.71	15.16	–	–	–
Dextran-iron oxide nanoparticles	39	58	93	21.26	20.90	19.78	2.00	4.19	4.62

the DSC, DTA and TGA. T_g values and the other parameters of DMA also supported to these results. The results of DMA demonstrated that the glass transition temperature of the composite increased with increase in concentration of nanoparticles. DMA results also showed an increase in storage modulus and decrease in tan δ consequently up on increasing the loading of filler in the dextran matrix. For the future aspects, examined and enlightened peculiarities of DIONPs can be used as potential biomedical materials due to the biocompatible and non-toxic nature.

Disclosure statement

The authors of the manuscript solemnly declare that no scientific and/or financial conflicts of interest, exists with other people or institutions.

References

[1] Zabihi O, Khodabandeh A, Ghasemlou S. Investigation of mechanical properties and cure behavior of DGEBA/nano-Fe_2O_3 with polyamine dendrimer. Polym Degrad Stab. 2012;97:1730–1736.

[2] Goiti E, Salinas MM, Arias G, et al. Effect of magnetic nanoparticles on the thermal properties of some hydrogels. Polym Degrad Stab. 2007;92:2198–2205.

[3] Laurent S, Forge D, Port M, et al. Magnetic iron oxide nanoparticles: synthesis, stabilization, vectorization, physicochemical characterizations, and biological applications. Chem Rev. 2010;4:2574–2574.

[4] Jain TK, Morales MA, Sahoo SK, et al. Iron oxide nanoparticles for sustained delivery of anticancer agents. Mol Pharm. 2005;2:194–205.

[5] Chourpa I, Douziech-Eyrolles L, Ngaboni-Okassa L, et al. Molecular composition of iron oxide nanoparticles, precursors for magnetic drug targeting, as characterized by confocal Raman microspectroscopy. Analyst. 2005;130:1395–1403.

[6] Dzunuzovic E, Marinovic-Cincovic M, Jeremic K, et al. Influence of a-Fe_2O_3 nanorods on the thermal stability of poly(methyl methacrylate) synthesized by in situ bulk polymerisation of methyl methacrylate. J Polym Degrad Stab. 2008;93:77–83.

[7] Modo M, Bulte JW. Cellular MR imaging. Mol Imaging. 2005;4:143–164.

[8] Bursa C, Laurent S, Roc A, et al. C-MALISA (cellular magnetic-linked immunosorbent assay), a new application of cellular ELISA for MRI. J Inorg Biochem. 2005;99:1135–1144.

[9] Mahdavi M, Bin Ahmad M, Haron MJ, et al. Synthesis, surface modification and characterization of biocompatible magnetic iron oxide nanoparticles for biomedical applications. Molecules. 2013;18:7533–7548.

[10] Kim DK, Zhang Y, Kehr J, et al. Characterization and MRI study of surfactant-coated superparamagnetic nanoparticles administered into the rat brain. J Magn Magn Mater. 2001;225:256–261.

[11] Nidhin M, Indumathy R, Sreeram KJ, et al. Synthesis of iron oxide nanoparticles of narrow size distribution on polysaccharide templates. J Bull Mater Sci. 2008;31:93–96.

[12] Hong RY, Feng B, Chen LL, et al. Synthesis, characterization and MRI application of dextran-coated Fe_3O_4 magnetic nanoparticles. Biochem Eng J. 2008;42:290–300.

[13] Li GY, Jiang Y, Huang K, et al. Preparation and properties of magnetic Fe_3O_4–chitosan nanoparticles. J Alloys Compd. 2008;466:451–456.

[14] Mukhopadhyay A, Joshi N, Chattopadhyay K, et al. A facile synthesis of PEG-coated magnetite (Fe_3O_4) nanoparticles and their prevention of the reduction of cytochrome C. ACS Appl Mater Interfaces. 2012;4:142–149.

[15] Molday RS, Mackenize D. Immunospecific ferromagnetic iron-dextran reagents for the labeling and magnetic separation of cells. J Immunol Methods. 1982;52:353–367.

[16] Weissleder R, Bogdanov A, Neuwelt EA, et al. Long-circulating iron oxides for MR imaging. Adv Drug Del Rev. 1995;16:321–334.

[17] Mukesh G, Harisinghani MG, Barentsz J, et al. Noninvasive detection of clinically occult lymph-node metastases in prostate cancer. N Engl J Med. 2003;384:2491–2499.

[18] Yu H, Fu G, Zhao J, et al. Synthesis and in vitro sorption properties of PAA-grafted cellulose beads for selective binding of LDL. Artif Cells Nanomed Biotechnol. 2006;34:501–513.

[19] Sehrig FZ, Majidi S, Asvadi S, et al. An update on clinical applications of magnetic nanoparticles for increasing the resolution of magnetic resonance imaging. Artif Cells Nanomed Biotechnol. 2016;44:1583–1158.

[20] Josephson L, Tung CH, Moore A, et al. High-efficiency intracellular magnetic labeling with novel superparamagnetic-Tat peptide conjugates. Bioconjugate Chem. 1999;10:186–191.

[21] Qu S, Yang H, Ren D, et al. Magnetite nanoparticles prepared by precipitation from partially reduced ferric chloride aqueous solutions. J Colloid Interface Sci. 1999;215:190–192.

[22] Wang X, Zhou J, Miao C, et al. Synthesis and size control of ferric oxide nanoparticles via a hydrothermal stripping route. J Nanopart Res. 2012;14:783.

[23] Bychko I, Kalishyn Y, Strizhak P. Size effect of Fe nanoparticles supported on carbon nanotubes on their activity and selectivity in the hydrogenation of crotonaldehyde. Adv Mater Phys Chem. 2012;2:17–22.

[24] Prakash A, McCormick AV, Zachariah MR. Aero-sol-gel synthesis of nanoporous iron-oxide particles: a potential oxidizer for nanoenergetic materials. Chem Mater. 2004;16:1466–1471.

[25] Hergt R, Dutz S, Muller R, et al. Magnetic particle hyperthermia: nanoparticle magnetism and materials development for cancer therapy. J Phys Condens Matter. 2006;18:2919–S2934.

[26] Darken LS, Gurry RW. The system iron—oxygen. II. Equilibrium and thermodynamics of liquid oxide and other phases. J Am Chem Soc. 1946;68:798–816.

[27] Wang SZ, Xin HW, Qian YT. Preparation of nanocrystalline Fe_3O_4 by γ-ray radiation. Mater Lett. 1997;33:113–116.

[28] Hong RY, Pan TT, Li HZ. Microwave synthesis of magnetic Fe_3O_4 nanoparticles used as a precursor of nanocomposites and ferrofluids. J Magn Magn Mater. 2006;303:60–68.

[29] Yu LQ, Zheng LJ, Yang JX. Study of preparation and properties on magnetization and stability for ferromagnetic fluids. Mater Chem Phys. 2000;66:6–9.

[30] Willard MA, Kurihara LK, Carpenter EE, et al. Chemically prepared magnetic nanoparticles. Int Mater Rev. 2004;49:125–170.

[31] Iconaru SL, Ciobanu CS, Le Coustumer P, et al. Structural characterization and magnetic properties of iron oxides biological polymers. J Supercond Nov Magn. 2013;26:851–855.

[32] Mathlouthi M, Koenig JL. Vibrational spectra of carbohydrates. Adv Carbohydr Chem Biochem. 1986;44:7–89.

[33] Hradil J, Pisarov A, Babic M, et al. Dextran-modified iron oxide nanoparticles. China Particuology. 2007;5:162–168.

[34] Wang HR, Chen KM. Preparation and surface active properties of biodegradable dextrin derivative surfactants. Colloids Surf A Phys Eng Asp. 2006;281:190–193.

[35] Predoi D. A study on iron oxide nanoparticles coated with dextrin obtained by coprecipitation. Dig J Nanomater Biostruct. 2007;2:169–173.

[36] Easo SL, Mohanan PV. Dextran stabilized iron oxide nanoparticles: synthesis, characterization and in vitro studies. Carbohydr Polym. 2013;92:726–732.

[37] Bautista MC, Miguel-Bomati O, Morales MP, et al. Surface characterisation of dextran-coated iron oxide nanoparticles prepared by laser pyrolysis and coprecipitation. J Magn Magn Mater. 2005;293:20–27.

[38] Thunemann AF, Schutt D. Maghemite nanoparticles protectively coated with poly (ethylene imine) and poly (ethylene oxide)-block-poly (glutamic acid). Langmuir. 2006;22:2351–2357.

[39] Taeghwan H. Chemical synthesis of magnetic nanoparticles. Chem Comm. 2003;8:927–934.

[40] Chen L, Li J, Lin Y, et al. Preparation of γ-Fe$_2$O$_3$/ZnFe$_2$O$_4$ nanoparticles by enhancement of surface modification with NaOH. Chem Cent J. 2014;8:40. doi: 10.1186/1752-153X-8-40.

[41] Kaplan Can H, Şahin Ö. Design, synthesis and characterization of 3,4-dihydro-2H-pyran containing copolymer/clay nanocomposites. J Macromol Sci A Pure Appl Chem. 2015;52:465–475.

[42] Gao L, Liu G, Hong RY, et al. Preparation and characterization of chitosan poly(acrylic acid) magnetic microspheres. Mar Drugs. 2010;8:2212–2222.

[43] Jurikova A, Csach K, Koneracka M, et al. Thermal analysis of magnetic nanoparticles modified with dextran. Acta Phys Pol A. 2012;121:1296–1298.

[44] Culita DC, Budrugeac P, Feder M, et al. Thermal analysis of two types of dextran-coated magnetite. J Therm Anal Calorim. 2010;101:181–187.

[45] Leslie-Pelecky DL, Rieke R. Magnetic properties of nanostructured materials. Chem Mater. 1996;8:1770–1783.

[46] Majetich SA, Jin Y. Magnetization directions of individual nanoparticles. Science. 1999;284:470–473.

[47] Stenekes RJH, De Semedt SC, Demeester J, et al. Pore sizes in hydrated dextran microspheres. Biomacromolecules. 2000;1:696–703.

[48] Turi EA. Thermal characterization of polymeric materials. 2nd ed. Brooklyn, NY: Academic Press; 1996, p. 980.